Egypt. J. Chem. **Vol. 68,** SI: Z. M. Nofal, pp. 561 - 574 (2025)

Egyptian Journal of Chemistry

http://ejchem.journals.ekb.eg/

Chitosan/ Sodium Alginate Scaffold Removes Fe from Underground Water and Combat Multidrug-resistant Bacteria

Gehad Z. Abdel-Hamed[a], Sawsan Dacrory[*b], Aly Al Sayed[c], Mohamed O. Abdel-Monem[a], Ghada E. Dawwam[a]

[a] *Botany and Microbiology Department, Faculty of Science, Benha University, Benha,13518, Egypt*

[b] *cellulose and Paper Department, National Research Centre, Dokki, Egypt.*

[c] *Water Pollution Research Department, National Research Centre, Dokki, Egypt*

Abstract

Underground water is an important source of drinking water worldwide. The occurrence of iron in water can cause staining, as well as unpleasant appearances and tastes. Therefore, in our study, we have formulated a 3D scaffold based on chitosan/ sodium alginate/ox. Cellulose/GO (Cs/SA/Ox. Cell/GO) has been prepared. Cellulose has been oxidized by TEMPO to make cellulose more reactive. Then ox.cellulose has been mixed with chitosan/ sodium alginate solution in the presence of different ratios of GO. The scaffolds have been investigated via FTIR, XRD, and SEM techniques. The prepared scaffold has been used for Fe^{+2}removal from underground water at different times, different pHs, and different dosages. The Antimicrobial activity of the prepared scaffold has been studied. Five pathogenic microorganisms were isolated from samples and identified by biochemical tests as *Pseudomonas aeroginosa*, *Neisseria* sp., *Klebsiella* sp., *Plesiomonasshigelloides*, and *Salmonella* sp. Composite 3 showed antimicrobial activity against a number of pathogenic microorganisms. The inhibition efficiency ranged between 12-25 mm. Thus, the prepared scaffold is considered a promising material for iron removal, besides having good antimicrobial activity.

Keywords: Chitosan- Graphene oxide- Adsorption- MDR bacteria- Antimicrobial activity

1. Introduction

Water is vital for all living organisms and constitutes about 71% of the Earth's surface. The total volume of water in the cosmos is constant, yet its use is rising at a rate more than double the pace of the world's human population. Accessing clean water has emerged as a significant concern in the 21st century, propelled by the rapid increase in water use, pollution, and shortage[1, 2]. The Earth's crust contains iron, which most abundant metallic element. Water infiltrating soil and rock can solubilize minerals, maintaining them in solution[3, 4].

These metallic elements are found in underground fluids, and certain surface waterways get significant groundwater input [5]. Iron is considered an indicator parameter, primarily composed of ingredients that are not typically of significant health issues. However, their occurrence in water can cause staining, as well as unpleasant appearances and tastes[6]. When exposed to air or oxygen, the dissolved iron oxidizes to Fe^{3+}, forming colloidal precipitates and making the water cloudy and turbid. The oxidation process is relatively slow, so the reduced forms can remain in aerated waters for a period of time. The occurrence of this metal in water presents a continuous challenge for water treatment [7].

Water is deemed unfit for human consumption when it contains harmful microorganisms. The bacteriological safety assessment of water relies on microbiologists' capacity to identify coliform bacteria in wells[8]. *Escherichia coli* is the predominant bacterium in the analysis, as it exhibits greater longevity in aquatic environments compared to other gut bacteria [9]. Pathogens such as *Escherichia coli*, *Shigella*sp., *Pseudomonas* sp., *Salmonella* sp., *Bacillus* sp., *Vibrio* sp., and *Streptococcus* sp. are bacterial groups implicated in disorders including diarrhea, enteric fever, dysentery, and other serious illnesses [10].

Commonly employed techniques for water treatment encompass coagulation, precipitation, adsorption, flocculation, complexation, reverse osmosis, ion exchange, electrocoagulation, electrodialysis, and catalytic processes (such as photocatalysis, UV photolysis, and advanced oxidation processes (AOPs)[11]. Filtration techniques using sand filter techniques have been applied for water treatment [12, 13].

Moreover, numerous materials, including natural and bio-based resources, have been recognized for application in water treatment [7, 14].

The adsorption method is a straightforward, economical, easy, and successful technique for treating contaminated wastewater. Common adsorbents, such as metal oxides, carbonaceous materials, and silica, are often employed to eliminate diverse contaminants [15]. Nonetheless, large-volume applications and continuous-flow water treatment systems are not a good fit for these adsorbents [16, 17]

*Corresponding author e-mail: sdmali82@yahoo.com.; (**Sawsan Dacrory**).

Received date 17 February 2025; Revised date 07 April 2025; Accepted date 13 April 2025

DOI: 10.21608/EJCHEM.2025.361424.11319

This study aims to investigate the impact of chitosan/sodium alginate/oxidized cellulose scaffold incorporated with different fractions of graphene oxide in the adsorption of iron from real underground water. The effect of contact time, pH, and composite dose on the adsorption process was investigated. The kinetic and isotherm studies were also carried out. In addition, isolation of pathogenic microorganisms from untreated groundwater and assessing the antimicrobial activity of the produced composite have been determined.

2. Experimental

2.1. Materials

Chitosan (Cs) with a deacetylation degree>90% was purchased from Sigma Aldrich. Graphene oxide (GO) was prepared and characterized according to previous work[18]. Bagasse raw material was sourced from the Quena Company of Paper Industry in Egypt. The chemical composition was ascertained in accordance with Tappi criteria T203, T211 (Klason lignin, pentosan, alpha cellulose, and ash content)[19]. The results were 22%, 44.4%, 28.1%, and 1.4%, respectively. Sodium alginate (SA) medium viscosity was purchased from Sigma Aldrich.TEMPO (2,2,6,6-tetramethylpiperidine-1-oxyl radical)was purchased fromBio Basic Canada Inc. All chemicals and reagents were analytical grade and used without further purification.

2.2. Fabrication of oxidized cellulose via TEMPO

Cellulose (5 g) was mixed with sodium bromide (0.8 g, 8 mmol) and TEMPO (0.08 g, 0.5 mmol) in 500 mL of distilled water then sodium hypochlorite solution (50 mL, 10%) was added and pH adjustment to 10 for 6h. at room temperature, the procedure concludes with a pH adjustment to 7
and centrifugation at 7000 rpm. The product underwent washing with water, dispersions, and centrifugation and subsequently dried at room temperature.

2.3. Fabrication of scaffold composite

A homogenous solution of Cs was prepared by dissolving 5g of Cs in 100 ml distilled water in the presence of 2% acetic acid with continued stirring. Then, 4 g of SA was dissolved in 100 mL distilled water to obtain a homogenous solution. The definite amounts of Cs and SA alongside the oxidized cellulose and GO in the mixture are given in Table 1.Subsequently the lyophilization process was carried out. After that, the composite was cross-linked by deepening in a $CaCl_2$ solution for 30 min. It was then washed with water and dried[16].

Table 1. Composition of the scaffold composite

Sample	Cs (g)	SA (g)	OCe (g)	GO (g)
Composite 1 (Cs/SA/OCe)	0.5	0.5	0.5	-
Composite 2 (Cs/SA/OCe)	0.5	0.5	0.5	0.1
Composite 3 (Cs/SA/OCe/GO)	0.5	0.5	0.5	0.2

2.4. Characterizations

FT-IR spectra were obtained within the range of 400–4000 cm−1 using a Shimadzu 8400S FT-IR Spectrophotometer. The surface morphology was examined utilizing an FEI IN SPECTS Company SEM electron microscope from Philips, Poland, employing environmental scanning without coating, alongside a JEOL JEM-2100 electron microscope at a magnification of 100,000x and an acceleration voltage of 120 kV. The XRD patterns were analyzed using a Diano X-ray diffractometer with a CuKα radiation source operating at 45 kV and a Philips X-ray diffractometer (PW 1930 generator, PW 1820 goniometer) with a CuK radiation source (λ=0.15418 nm), over a diffraction angle range of 2θ from 10 to 80° in reflection mode and the crystalinity has calculated from the equation .

$$CrI = \frac{(I_{002} - I_{am})}{I_{002}} \times 100$$

Where I_{002} and I_{am} are the maximum intensity of the 002 lattice diffraction and lam is the intensity of diffraction in the same units at 28 = 18°.

2.5. Study Area and Collection of Samples

The research was conducted from groundwater Egypt. Six water samples were obtained (S1, S2, S3, S4, S5, S6). The samples were collected from various locations within. The physical and chemical evaluations of several water samples are presented in Table 2.

2.5.1. Physicochemical properties of samples

The pH of each water sample was measured in situ and documented throughout the sampling procedure with a digital meter (METTLER TOLEDO). Temperature measurements for each water sample were acquired and documented utilizing a digital

meter (JENWAY, 4510 Conductivity meter). The electrical conductivity of each water sample was measured in situ with a digital meter (JENWAY, 4510 Conductivity meter). The turbidity of the water samples was evaluated using a calibrated turbidity meter (HACH, TL2300) employing the nephelometric method, which quantifies the intensity of scattered light. The samples were gathered in sterile, sealed containers and let to settle prior to measurement. Turbidity was measured in nephelometric turbidity units (NTU) to quantify suspended particle concentration and evaluate water quality (Patil et al., 2012). All readings were documented appropriately.
The amounts of chloride, water hardness, alkalinity, and iron in the collected water samples were ascertained using the methodology outlined by Baird et al. (2017)[22].

Sorption studies

2.5.2. composite comparative study

The optimum removal efficiency of the prepared scaffold composites has been studied as follows. 50 mL of 100 mg/L Fe solution was added to the prepared composites. The mixture was shaken for 120 min, then the solution was filtered, and the Fe ion concentration was measured by. The removal efficiency (*R%*) and the amount of Fe ion uptakes (q_e) by the sorbent were calculated using equations 1 and 2:

$$R\,\% = \frac{C_o - C_t}{C_o} X\ 100 \qquad (1)$$

$$\mathrm{q_e} = (C_o - C_t)\mathrm{X}\frac{\mathrm{V}}{\mathrm{M}} \qquad (2)$$

where; C_o and C_t are the initial and remaining concentration of Fe ion (mg/L) at different time (t). V is the volume of solution (mL), and M is the composite mass (g).

2.5.3. Effect of pH on the adsorption

Influence of various pH (2–12) on the removal efficiency was studied using 0.2 g of scaffold composite and 50 mg/L of Fe ion. 0.1N NaOH and 0.1N HCl were used to adjust the tested solution pH. Then, the removal % of Fe ion from the tested solutions after 120 min was measured.

2.5.4. Effect of time on the adsorption

The contact time effect on the removal efficiency was estimated by adding 0.2 g of composite to 50 mL of Fe ion solution under shaking for a different time (30–120 min) at 25 °C.At each time point, a 3 ml sample was taken from the same solution for analysis.

2.3.2. Effect of composite dose on the adsorption

Effect of composite dose variation (0.05-0.2g) on the adsorption efficiency of 50 mL Fe ion at pH =10 for 120 min. has been studied.

2.5.5. ***Adsorption kinetic and isotherm***

Sorption kinetics of Fe ion from aqueous solution was illustrated by pseudo-first-order, pseudo-second-order, and intra-particle diffusion (Eqs 3, 4, and 5, respectively).

$$\log(q_e - q_t) = \log(q_e) - \frac{K_1}{22.303}t \quad (3)$$

$$\frac{t}{q_e} = \frac{t}{q_e} + \frac{1}{K_2 q_e{}^2} \quad (4)$$

$$q_t = \mathrm{k_p(t)^{0.5} + C} \qquad (5)$$

Where q_t and q_e represent the adsorption capacities of Fe ions (mg/g) at time t and at equilibrium, respectively, and k_1 denotes the rate constant of pseudo-first-order adsorption (min−1). $k_2$represents the rate constant for pseudo-second-order sorption (g/mg min). The plots of t/q_t against t produced a linear representation [35]. The adsorption parameters q_e and k_2 were ascertained from the slope and intercept of the plot, respectively. K_p represents the intraparticle diffusion rate constant, whereas C is the intercept of the intraparticle diffusion graph. The value of k_p was determined from the slope of the $q_t$vs t0.5 plot. The intraparticle diffusion model elucidates the mechanisms and rate-controlling processes in the kinetics of biosorption[11].

2.5.6. Iron determination

The Fe ion concentration was determined by using the methodology outlined by Ric et al.[22]. In brief, to 50ml of water sample, 1 ml of ammonium hydroxide and 2 ml conc. HCL were added. Then the solution was heated until concentrated to 25 ml, then 10 ml ammonium acetate and 4 ml of 1,10phenanthrolin reagent (phenanthrolinmehode) according to Standrd method were added, completed to 50 ml with dist. water and read on spectrophotometer at 510 nm.

2.6. Microbiological Assessment of collected Water Samples

2.6.1. Enumeration of total viable bacteria

One milliliter of water samples was incorporated into Reasoner's 2A (R2A) agar plates medium. The plates were incubated for 48 hours at 35 °C. The bacterial count was measured in cfu/ml.

2.6.2. Multiple-tube fermentation technique

a. Presumptive Phase

Lauryl tryptose broth triple-strength media was utilized in this phase of the multiple-tube test following the methodology of Dawwam et al.[23].Fermentation tubes were stacked in rows of five within a test tube rack. Twenty milliliters of water samples were inoculated into ten milliliters of lauryl tryptose broth. The tubes were gently agitated and incubated at 35 ± 0.5°C for 48 ± 2 hours. Following the incubation period, the tubes were agitated and assessed for growth, turbidity, and acidic response, indicated by varying colors of yellow. Positive tubes were allocated to the verified test.

b. Confirmed Phase

All presumptive tubes exhibiting growth and turbidity, any quantity of gas, or acidic response within 24 ± 2 hours of incubation were taken to the confirmation phase. Brilliant green lactose bile (BGLB) broth fermentation tubes were utilized for the confirmation phase. A sterile loop was utilized to transfer one or more loopfuls of culture to a fermentation tube with BGLB broth. Injured BGLB broth tubes were incubated at 35 ± 0.5°C. Any gas produced in the inverted vial of the BGLB broth fermentation tube at any point within 48 ± 3 hours signifies a verified positive phase[18].

2.6.3. Isolation and Biochemical Characterization of Bacterial Isolates

A loopful of cultures from several samples cultivated on R2A agar medium was transferred to nutrient agar medium. Then the plates were incubated for 24 to 48 hours at 37 °C.

The phenotypic characterization of bacterial isolates was conducted using morphological and biochemical assessments as outlined in Bergey's Manual of Systematic Bacteriology[25]. Morphological characteristics, including shape, Gram staining, and colony morphology, were examined by a light compound microscope. Biochemical characterizations, including indole was determined by Dawwam et al. [26]. Other biochemical tests as citrate, urease, triple sugar iron, lysine iron agar, and catalase assays were conducted as outlined by Holt et al [25].

2.6.4. Antibiotic Susceptibility Testing

The inoculum of each bacterial isolate was cultivated and disseminated on Mueller–Hinton agar plates. The antibiotic discs were positioned on the agar plates and incubated overnight at 37 °C for 24 hours. The inhibition zones were assessed, and the isolates were categorized as sensitive, moderately sensitive, or resistant based on CLSI tables and recommendations.

Antibiotic susceptibility test was conducted utilizing the disc diffusion technique [20]for the indicated antibiotics, Piperacillin- tazobactam(TPZ), Amikacin (AK), Tigecyclin (TGC), Ceftrixone (CRO),Ceftazidine (CAZ), Ampicillin-Sulbactam (SAM), Levofloxacin (Levo), Cefoxitin (FOX), Amoxicillin- Clavularat (AMC), Cefatoxime (CTX), Gentamycin (CN), , Ertapenem (ETP), Meropenem (MRP), Ciprofloxacin (CIP), Aztreonam (ATM), and, Sujphamethazole-Trimethoprim(SXT), Fosfomycin(FO), Doxycuclin(DO), Clarythromycin(CIR), Colistin(CI), Linezolid(LZD), Kanamycin(K), Cefepime(CPM) and Imipenem(IPM).

2.6.5. Antimicrobial test

The antimicrobial efficacy of the composite under investigation was evaluated against Gram-positive bacteria (*Staphylococcus aureus* ATCC 43300, *Listeria monocytogenes* ATCC 19155), Gram-negative bacteria (*Salmonella* sp. ATCC 14028, *E. coli* ATCC 8739, *Pseudomonas aeruginosa, Neisseria* sp., *Klebsiella* sp., and *Blesiomonasshigelloides*), and unicellular fungi (*Candida albicans* ATCC 10231) employing the agar diffusion technique as per Al-Shemy et al[21]. The bacteria were grown in a nutrient-liquid medium on a shaker platform at 200 rpm for 24 hours at 37 °C. Bacteria (1.5×10^8 CFU) were inoculated into Mueller-Hinton agar plates; thereafter, 200 µL of the material under investigation was introduced into wells (7 mm in diameter) excised from the agar plates. Agar plates were incubated at 37 °C for 24 hours. All investigations were performed in triplicate for each tested strain. The inhibitory zones surrounding the discs were measured in millimeters.

3. Result and discussion

3.1. Charcterization of fabricated materials

3.1.1. FTIR analysis

FTIR is a specific tool to identify the functional groups in the materials under investigation. **Figure 1A.** shows FTIR analysis of neat cellulose, oxidized cellulose (OCe), and chitosan (Cs) materials. Cellulose showed characteristic adsorption bands related to the fingerprint of cellulose I structure. The wide peak between frequencies of 3000–3500 cm^{-1} corresponds to OH stretching, while the peak at 2900 cm^{-1} corresponds to CH stretching, the peak at 1650 cm^{-1} due to C=Oabsorbed water and ether linkage C-O-C ensued at 1100 cm^{-1}. Unlike, the intensity of these peaks in OCe decreased upon TEMPO oxidation due to the destruction of hydrogen bonding in the cellulose chain [29].Cs shows different peaks at 3500 cm^{-1} corresponding to OH stretching vibration with NH_2 2900 cm^{-1} due to CH vibration, 1660 cm^{-1} for C=O of amide group, 1340 cm^{-1} due to C-N, and at 1050 cm^{-1} ether linkage C-O-C. **Figure 1B** shows FTIR of the prepared scaffold composite. Two passable interactions occurred: a) physical interaction and Schiff base interaction between NH_2 of Cs and C=O of OCs. The main peaks appeared at 3500cm^{-1}, 1600 cm^{-1} and 1100 cm^{-1} due to OH stretching, C=O of amide and ether linkage [2, 30].

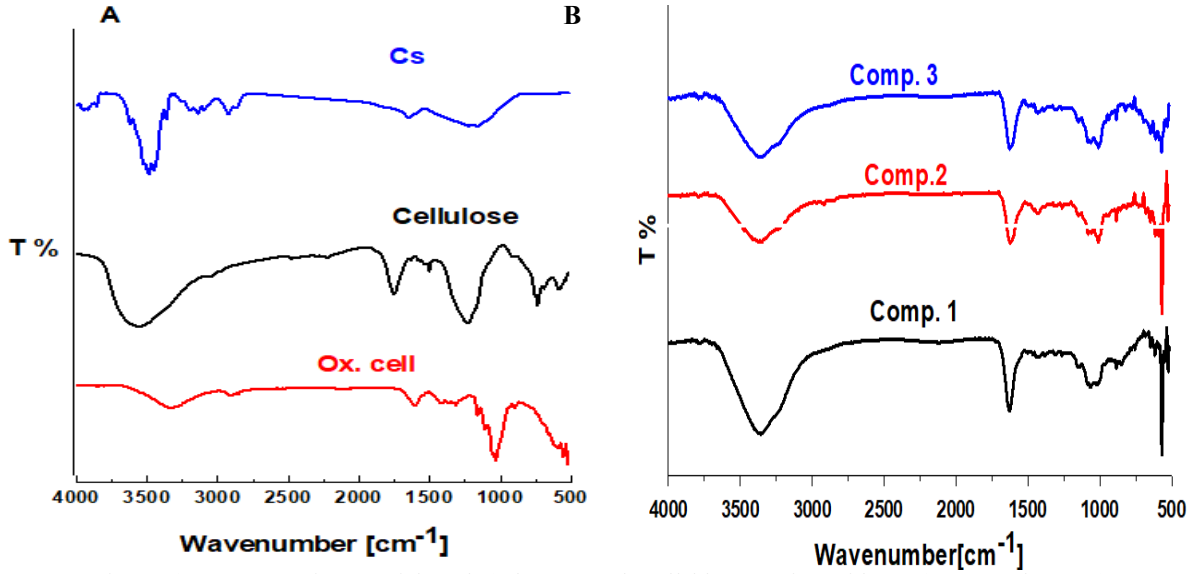

Fig. 1. A) neat composite materials and B) the prepared scaffold composites with GO (0, 0.1, and 0.2 gm).

3.1.2. Scanning electron microscope (SEM)

Figure 2 shows the surface morphology of Cs, OCe, and the prepared composite. Cs appears as a small sheet-paper smooth and homogenous, while OCe appears as compact fibers collected together. The prepared composites 1 and 3 appear as compacted layers of films with some embedded fibers.

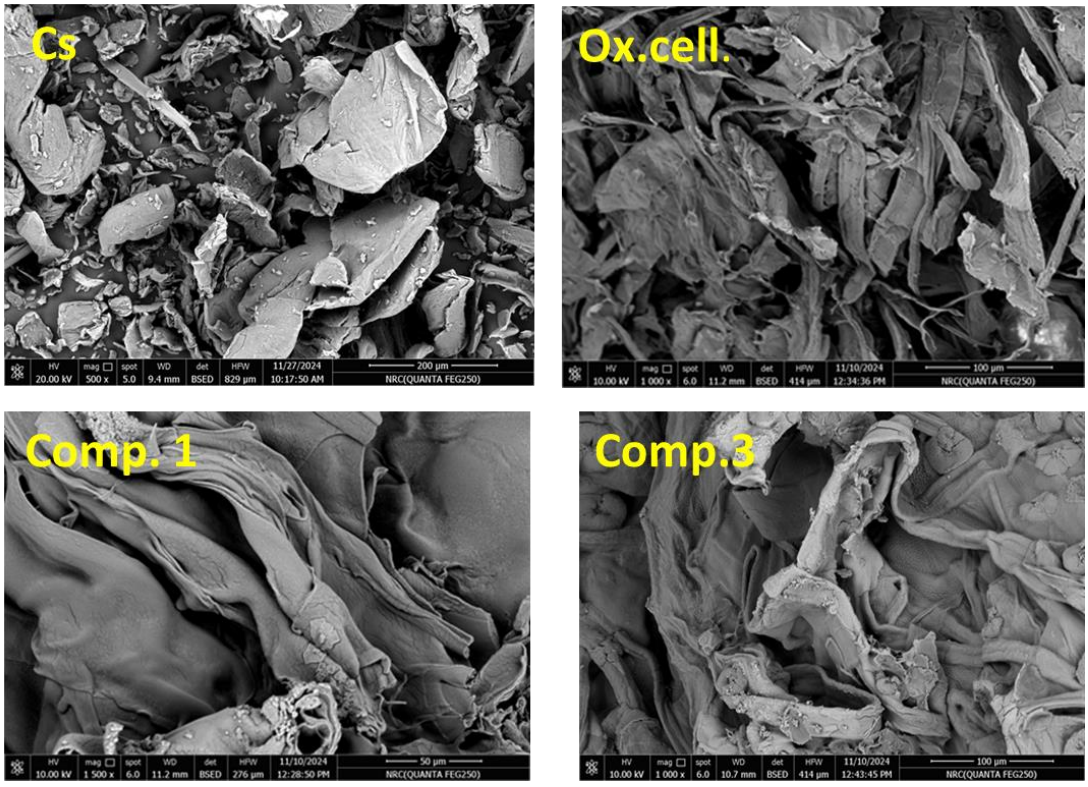

Fig. 2. SEM of Cs, OCe, and the prepared scaffold composites (comp. 1=blank & comp. 3=0.2g GO).

3.1.3. X-ray diffraction

Figure 3 illustrates the x-ray pattern of Cs, cellulose, OCe, and the prepared composites. Cellulose pattern shows two peaks at 2θ = 15 and 16.5°, sharp peak at 2θ = 22°, and weak peak at 2θ = 34° [29]. The reduction of crystallinity upon TEMPO oxidation is evidence of the hydrogen bond destruction taking place during the oxidation process where cellulose CrI= 75% and became 67% after TEMPO. Cs XRD pattern shows the semi-crystalline characteristic peaks at 2θ = 10°, 23°, and 45°.

From **Figure 3B**, all the neat composite materials' characteristic peaks have disappeared in the prepared composite, which confirms the compatibility and bonding between them in the fabricated scaffolds [4]. **Figure 3C** shows XRD pattern GO with a distinctive peak at 2θ = 10, and SA pattern with peak at 2θ =15 , 25°.

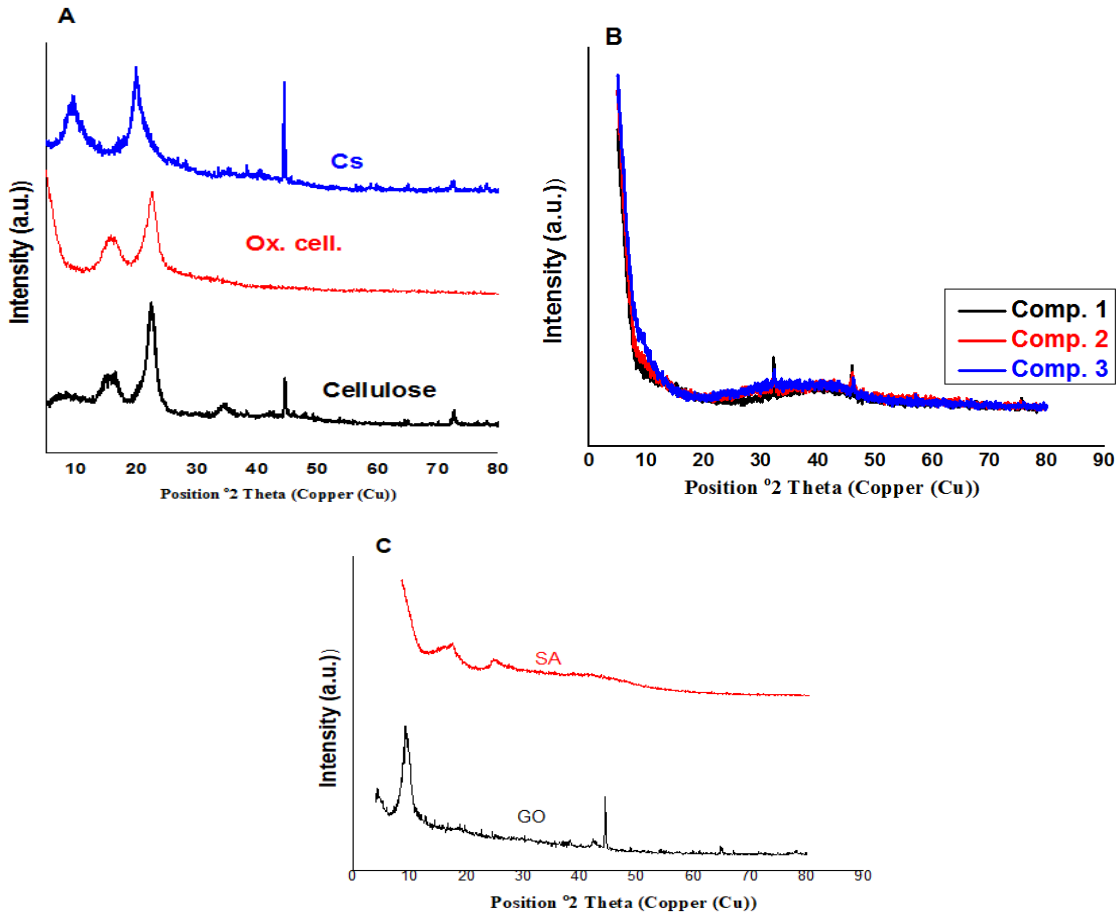

Fig. 3. XRD of A) Neat composite materials and B) The prepared scaffold composites with GO (0, 0.1, and 0.2 g) C) SA and GO .

3.2. Physicochemical parameters of collected samples

Physical and chemical analyses of different water samples were determined as shown in **Table 2.**

Table 2. Physicochemical parameters of collected samples

Physiochemical parameters	Unit	Standard* Limit	Samples Code					
			S1	S2	S3	S4	S5	S6
Turbidity	NTU	>1	2	7	3.5	0.8	13	10
pH	-	6.5-8.5	7.8	7.6	7.8	7.6	7.7	7.7
EC(Electrical conductivity)	Ms	-	868	776	836	887	972	1211
TDS(Total dissolved Solids)	mg/L	<1000	572	512	551	585	641	799
Temperature	℃	-	20.6	21.9	21.5	20.2	21.3	21.8
Chloride	mg /L	<250	150	98	132	149	130	170
Total Hardness	mg/L	<500	420	420	440	440	480	660
Calcium Hardness	mg /L	<500	300	260	280	300	300	340
Magnesium Hardness	mg/L	>150	120	160	160	140	180	320
Alkalinity	mg/L	-	380	380	400	400	400	660

The **pH** of water samples varied across different sites. Samples collected from various locations showed pH values within the acceptable range set by the WHO [31] (6.5 – 8.5). This result corresponds with the conclusions of Ayandiran et al.[32]. Research indicates that low pH levels (between 3 and 5) markedly diminish bacterial population, variety, and activity, potentially eradicating antibiotic-resistant organisms (Yu et al.,)[33]. Conversely, Gama et al.[34]. indicated that elevated pH levels correlated with an increase in bacterial diversity, antibiotic resistance, and population density.
For **temperature,** the recorded temperature ranges (20.2 – 21.9 °C) of all the sample sites indicated a favorable environmental condition that enhanced the mesophilic bacteria. In this regard, Isnawati*et al.*[35] stated that microbes that can grow at optimal temperatures are called mesophilic bacteria.
The electrical conductivity (EC) and salt levels varied from one sample to another in the range from 776 to 1211 µS/cm.Ateba*et al*. [36]found that Law electrical conductivity levels reduce the concentration of dissolved salts, which in turn leads to a decreased bacterial load [37] assert that bacterial diversity is not influenced by fluctuations in water salinity, attributable to the bacteria's exceptional genetic flexibility and salt tolerance methods. Bacterial abundance may remain unaffected despite variations in salt levels. Likewise, concerning antibiotic resistance, elevated salinity has been associated with the suppression of growth in some bacteria harboring antibiotic resistance genes (ARGs) [38]. All samples showed a higher limited range of turbidity, which exceeded 1.0 NTU except sample Number 4, which represents 0.8 NTU. According to WHO, turbidity in water can signal the existence of pathogenic microorganisms, including bacteria, viruses, and parasites. These pathogens may lead to symptoms such as nausea, cramps, diarrhea, and headaches.

The total alkalinity range set by WHO is 500 mg/L. Our results showed that the alkalinity of all samples is in accordance with standard data that represented values lower than 500 mg/l except, sample No.6 which recorded a higher than standard value (660 mg/l). Water hardness measured in all samples showed normal results except sample Number 6 (660 mg/l) which exceeds the limited value according to WHO.

3.3. Sorption Study

3.3.1. Effect of pH

pH value is the most important aspect that effect on the adsorption capacity. Figure 4 shows the adsorption capacity of 0.2g of composite 3 at pH range (2-10) towards 50 mg/L Fe^{+2}. It illustrates that the adsorption capacity is pH dependent. The adsorption increase with increasing pH until reach 60% at pH=10, wherethe composite ionization increase and enhance chelate formation with Fe^{2+}.

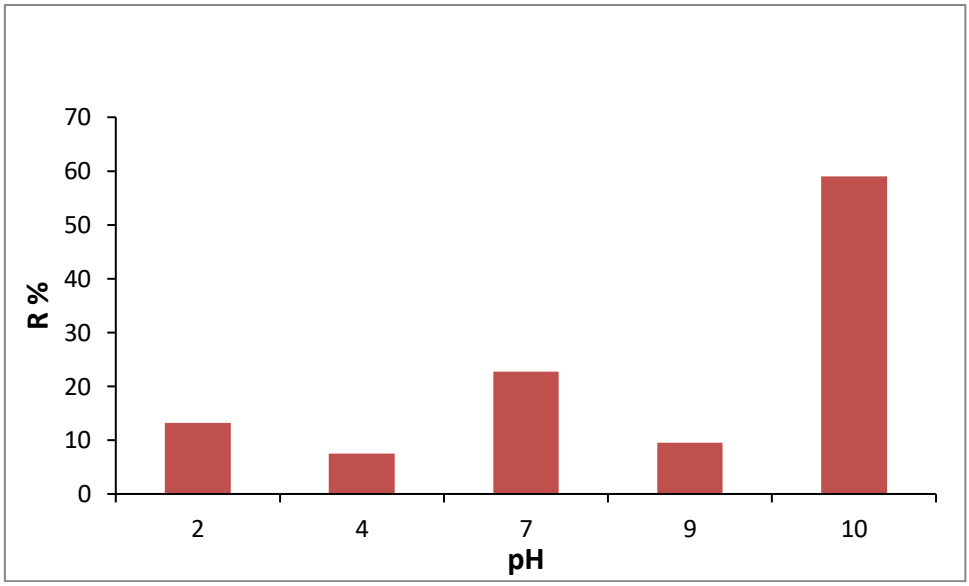

Fig. 4. Effect of pH on removal % of Fe^{+2} using 0.2 g of composite to 50 mL of Fe^{+2} solution under shaking for 120 min. at 25 °C.

3.3.2. Effect of time

Figure 5A shows the effect of time on adsorption capacity, where the adsorption increases with time until it reaches a stable point of equilibrium. This behavior could be due to the increase of active moieties such as COO^- and OH that are capable of making chelation on the surface, but with time, most of these sites became occupied with Fe^{+2}. The pseudo-first- and second-order has been employed to investigate the kinetics of adsorption.

From **Figure 5B** the adsorption fits the pseudo-first-order with a correlation coefficient R= 0.957 thus the adsorption process is likely to occur via a physisorption reaction that depends on the diffusion process. This hypothesis is manifested clearly in the intra-particle diffusion model as in **Figure 5C.**

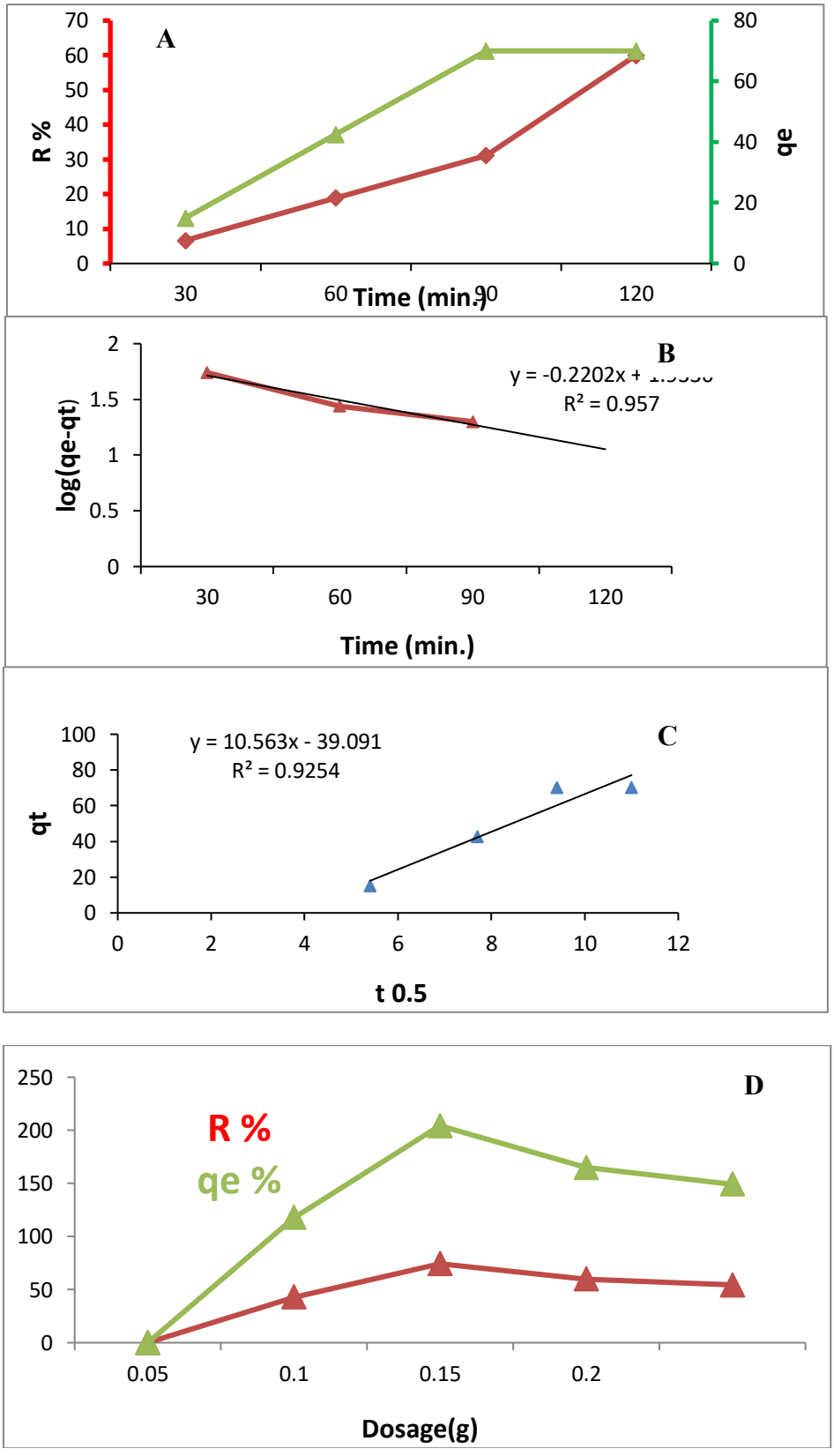

Fig. 5. (A) Impact of contact time, (B) pseudo 1st order kinetic plot, (C) intra-particle diffusion plot and D) effect of dosage for the Fe^{+2} adsorption by 0.2 g of composite 3 in 50 mL of Fe^{+2}solution for a different time (30–120 min.) at 25 °C and pH =10.

3.3.3. Effect of dosage on the adsorption process

The sorbent dosage used to remove Fe^{+2} from ground water is an essential factor. **Figure 5D** shows the effect of composite 3 doses (0.05 - 0.2 g) on the removal efficiency (R) and the uptake capacity (q). As the dose increased, the removal efficiency increased due to increase the surface sites that can adsorb Fe^{+2} ions.

3.4. Enumeration of Total Viable Bacteria

Water is important for life on Earth but it can also serve as an ideal environment for various pathogens. Data in **Table 3.**Shows the colony forming unit per millimeter for different organisms isolated on R2A agar media from different untreated groundwater. The untreated groundwater included a great number of total bacterial counts that are greater than 50 cfu/ml indicating microbial contamination of water.

The highest average was observed in the S2 sample equal to 400 cfu/ml and the lowest average in sample 5 which counts 90 cfu/ ml.

Contaminated drinking water and poor sanitation conditions increase the risk of various health hazards, including typhoid fever, shigellosis, and other diseases.

Consistent with the World Health Organization, 60% of all diarrhea-related deaths in low- and middle-income countries are linked to insufficient access to clean drinking water (35%), inadequate sanitation (31%), and poor hygiene practices (12%).

Table 3. The average number of colony-forming unit (cfu/ml) for different collected samples.

Location	CFU/ml
S1	100
S2	400
S3	125
S4	110
S5	90
S6	140

3.5. Multiple-Tube Fermentation Technique

A lactose-based broth medium was employed to identify the metabolic byproducts of lactose fermentation. The bacterial density can be calculated using the provided formula or by referencing the table based on the count of positive tubes in the numerous dilutions. MPN Index/100 ml for tested isolates was recorded according to data in **Table 4.**

Table 4. MPN index and 95% confidence limits for different combinations of positive and negative results when utilizing five 20 ml portions (APHA, 1992).

NO. of Tubes Giving Positive Reaction Out of 5 of 20 ml Each	MPN Index/100 ml	95%Confidence Limits (Approximate)	
		Lower	Upper
0	**<1.1**	**0**	**3.0**
1	**1.1**	**0.05**	**6.3**
2	**2.6**	**0.3**	**9.6**
3	**4.6**	**0.8**	**14.7**
4	**8**	**1.7**	**26.4**
5	**>8**	**4.0**	**Infinite**

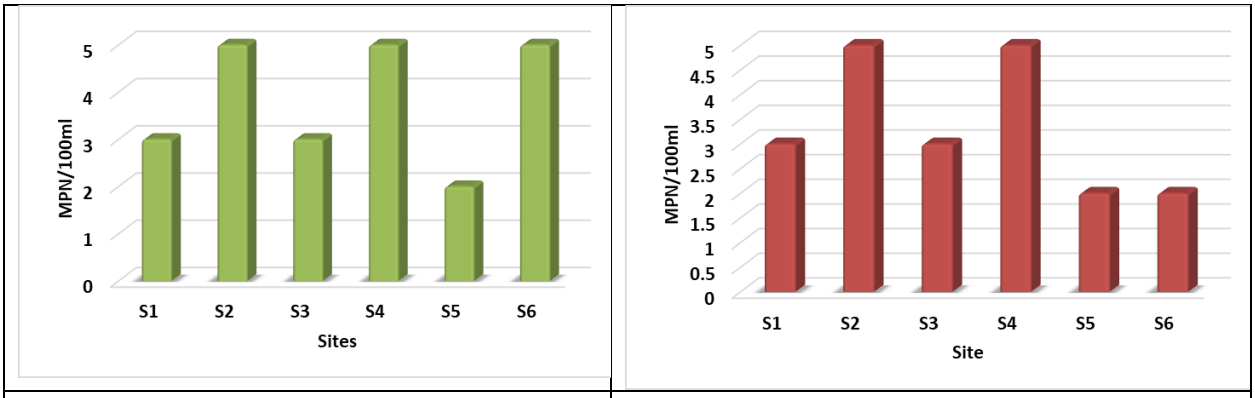

Fig. 6. Results of (A) Presumptive test and (B) confirmed test for different collected samples.

Results of the presumptive test showed that Samples number (2, 4, and 6) >8 MPN index /100 ml. while S1, S3, and S5 gave 4.6, 4.6 and 2.6 MPN index /100 ml respectively (**Fig 6A**). Results of the confirmed test showed that S2 and S4 gave 8 MPN index /100 ml while S1, and S3 gave 4.6 MPN index /100 ml. In addition, S5 and S6 gave 2.6 MPN index /100 ml (**Fig 6B**).

3.6. **Isolation of bacterial isolates**

Five different bacterial isolates were obtained from the six collected water samples. The isolates took the codes P1 to P5.

3.6.1. **Morphological and biochemical characterization of bacterial isolates**

The morphological and biochemical tests are shown in **Table 5.** Microscopic morphology confirmed that all isolates were gram-negative bacilli. All isolates were indole negative Also, all isolates were catalase negative except P1 and P3 were positive. Additionally, all isolates were urease positive except P5 which was negative while all isolates were oxidase positive except P3 was negative. All isolates were LIA-positive.

According to the citrate test P1, P2, and P4 represent negative citrate whereas P3 and P5 showed positive citrate. Also, the tabulated data illustrates K/K in TSI with P1, P2, and P3 while, P4 showed K/A and, P5 represented A/A with H_2S gases which give black color.
According to biochemical identification**,**isolates P1, P2, P3, P4, and P5 may be identified as *Pseudomonas aeroginosa*, *Neisseria* sp., *Klebsiella* sp., *Plesiomonasshigelloides*, and *Salmonella* sp., respectively.

Biochemical tests such as urease test, oxidase test, and indole test are used for the identification of Gram-negative bacteria (Muhammad Shoaib*etal*,)[39]In this regard, Abdeltawab*et al*. [40]approved that *Salmonella* sp. gives a positive LIA test and is significant with the production of H_2S gas in the TSI test whereas it gives negative results with indole and urease tests.
Also,[28] agreed with *Salmonella* in citrate and urease tests.
In addition [29] confirmed that all *P. aeruginosa* isolates gave positive results for catalase and oxidase tests. About *Klebsiella* sp., approved that *Klebsiella* showed positive catalase, citrate, and urease test and negative oxidase and indole tests. Also, Rawy*et al*.[30] showed that*Klebsiella pneumonia* is oxidase-negative, indole-negative, and urease-positive.
Plesiomonasshigelloides are members of the family Enterobacteriaceae and give positive oxidase test[31]. Furthermore, *Neisseria* sp. are gram-negative bacteria that showed positive oxidase test as determined by[32] while*pseudomonasaeruginosa* was positive for oxidase, catalase and negative for indole tests[33].

Table 5. Morphological and biochemical tests for different bacterial isolates

Isolate Number	Gram staining	Bacterial shape	TSI	LIA	Indole	Urease	Citrate	Identified organism may be
P1	Negative	Bacilli	K / K	+Ve	-Ve	+Ve	-Ve	*Pesudomonasaeruginosa*
P2	Negative	Bacilli	K / K	+Ve	-Ve	+Ve	-Ve	*Neisseria* sp.
P3	Negative	Bacilli	K / K	+Ve	-Ve	+Ve	+Ve	*Klebsiella*sp.
P4	Negative	Bacilli	K / A	+Ve	-Ve	+Ve	-Ve	*Plesiomonasshigelloides*
P5	Negative	Bacilli	A/A $+H_2S$	+Ve	-Ve	-Ve	+Ve	*Salmonella* sp.

*A: acidic, k: Alkaline, -: negative, +: positive.

3.6.2. Antibiotic Susceptibility of The Bacterial Isolates

Previous investigations have indicated that antibiotic-resistant bacteria are widely distributed in surface and ground waters [34, 35]). Data in **Table 5** showed the resistance/sensitivity of the isolated microbes toward twenty-four popular antibiotics. The isolated *Neisseria* sp. is highly sensitive to nineteen antibiotics and resistant to four antibiotics.
All organisms were sensitive to eleven antibiotics and resistant to three, while *plesiomonasshigelloids*was sensitive to fourteen antibiotics and highly resistant to nine antibiotics.

Table 6. Resistance/ sensitivity of the isolated bacteria to different antibiotics

Antibiotics	Concentrations (*Mg*/disc)	Antibiotic susceptibility pattern				
		Pesudomonas aeruginosa	Neisseria	Klebsiella	Plesiomonas shigelloides	Salmonella
Gentamycin	10	S	S	S	S	S
Doxycycline	30	S	S	S	S	S
Levofloxacin	5	S	S	S	S	S
Fosfomycin	200	R	S	R	R	S
Sulphamethazole-trimethoprim	25	WS	S	S	WS	WS
Teigycycline	15	S	S	S	S	S
Ciprofloxacin	20	S	S	S	S	S
Aztreonam		R	R	R	R	R
Piperacillin-tazobactam		S	S	S	S	S
Imipenem	10	S	S	S	S	S
Ceftazidine	30	R	R	R	R	R
Ampicillin-Sulbactam		S	S	S	S	R
Cefepime		WS	S	WS	WS	R
Amoxicillin- Clavularat	30	S	S	S	S	WS
Cefoxitin	30	S	S	S	S	WS
Cefatoxime	30	WS	R	R	WS	R
Ceftrixone	30	R	R	R	R	R
Ertapenem)	10	S	S	S	S	S
Colistin		S	WS	R	S	R
Kanamycin	30	S	S	S	S	S
Linezolid	30	S	S	S	S	R
Meropenem		S	S	S	S	S
Amikacin	30	S	S	S	S	S
Clarythromycin	15	R	S	S	R	S

* R: resistant, S: sensitive, WS:weak sensitive

Previous studies have reported microorganisms' resistance to clinically relevant antibiotics[36, 37]. Various authors isolated E. coli, Shigella, and Salmonella from water samples[38, 39]. This study was motivated by the prevalence of reports regarding pathogenic microorganisms in drinking water and related diseases[40].

Resistance may be linked to significant contamination from sewage effluent, surface runoff, agricultural practices, wildlife, and industrial pollution. This study's findings regarding bacterial resistance profiles align with earlier research conducted in various surface and drinking water systems [41].

This study confirmed that the prevalence of pathogenic bacteria in well water may result from inadequate sanitation, the mixing of sewage effluents with well water, and fecal contamination. In Pakistan, 74% of tape, storage tanks, and tube wells were found to be contaminated with E. coli, followed by Salmonella spp. at 54% and Shigella spp. at 40% . Therefore, it is essential to monitor pathogenic bacteria and adhere to WHO standards for drinking water.

3.7. Antimicrobial Activity

Data in Fig.7.shows that composite 3 has antimicrobial activity against a number of pathogenic microorganisms. The inhibition efficiency ranged between 12-25 mm. The highest inhibition efficiency was observed for *Neisseria* sp.
Chitosan has potent antibacterial properties and is safe for human consumption. Numerous publications examine the antibacterial efficacy of chitosan under various situations. The findings indicated that the antibacterial efficacy is enhanced for chitosan with reduced molecular weights (MW)[42]. Chitosan is a cationic molecule whose antimicrobial mechanism targets the anionic bacterial cell wall, leading to the disruption of membrane functions, such as facilitating the leakage of intracellular constituents and impeding nutrient transport into the cells.

Furthermore, GO is engaged with bacteria by a cell entrapment mechanism, wherein the antibacterial efficacy of GO is augmented with the expansion of sheet area.

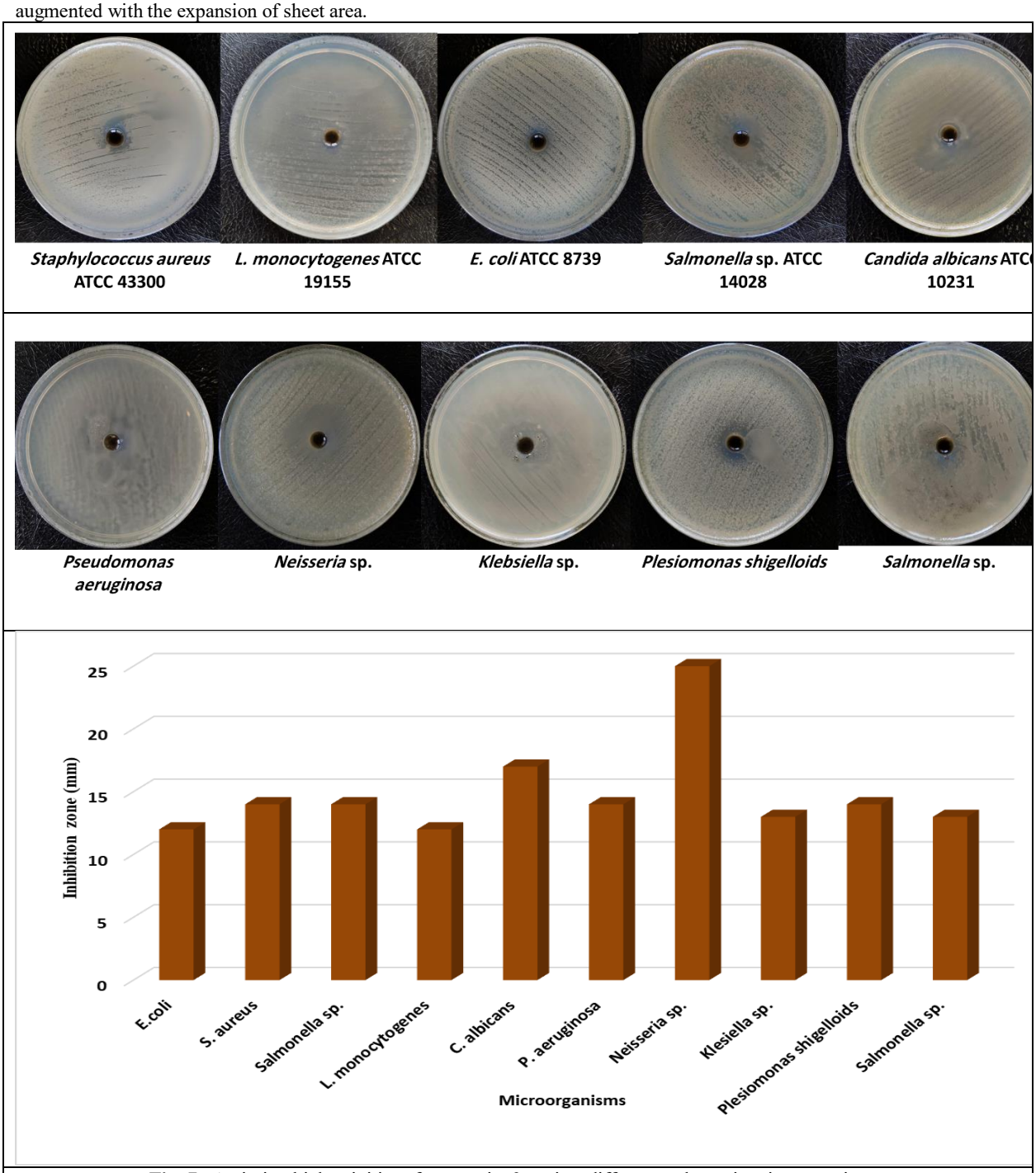

Fig. 7. Antimicrobial activities of composite 3 against different pathogenic microorganisms.

4. Conclusions

Chitosan /sodium alginate/oxidized cellulose scaffold incorporated with different fractions of graphene oxide has been fabricated and investigated via FTIR, XRD, and SEM. The scaffold showed efficiency in the adsorption of iron from real underground water at different times, different pHs, and different dosages. Moreover, the prepared composite has shown antimicrobial activity against a number of pathogenic microorganisms that have been isolated from untreated groundwater, in addition to other multidrug-resistant microbes. These results enable us to suggest the novel Chitosan/sodium alginate/oxidized cellulose scaffold as a material with promise for iron removal and combating pathogenic microorganisms in underground water.

Declaration of competing interest

The authors declare that they have no known competing financial interests or personal relationships that could have appeared to influence the work reported in this article.

Acknowledgments

The author would like to acknowledge National Research Centre, Egypt and Faculty of Science, Benha University for financial support for this research.

References

1. Abdelhamid, H.N., *Nanocellulose-based materials for water pollutant removal: A review.* International Journal of Molecular Sciences, 2024. **25**(15): p. 8529.
2. D'Amora, U., et al., *Advances in the physico-chemical, antimicrobial and angiogenic properties of graphene-oxide/cellulose nanocomposites for wound healing.* Pharmaceutics, 2023. **15**(2): p. 338.
3. Dvorak, B.I., S.O. Skipton, and W. Woldt, *Drinking water: iron and manganese.* NebGuide œ University of NebraskaœLincoln Extension Publications G, 2007. **1714**.
4. El-Sayed, E.S.A., et al., *Sustainable grafted chitosan-dialdehyde cellulose with high adsorption capacity of heavy metal.* BMC chemistry, 2023. **17**(1): p. 117.
5. Casey, T., *Iron and manganese in water: Occurrence, drinking water standards, treatment options.* Aquavarra Research Publications Water Engineering Papers, 2009. **3**: p. 1-6.
6. Wu, S., et al., *Recent advances on sustainable bio-based materials for water treatment: Fabrication, modification and application.* Journal of Environmental Chemical Engineering, 2022. **10**(6): p. 108921.
7. Abouzeid, R.E., M.E. Owda, and S. Dacrory, *Effective adsorption of cationic methylene blue dye on cellulose nanofiber/graphene oxide/silica nanocomposite: Kinetics and equilibrium.* Journal of Applied Polymer Science, 2022. **139**(25): p. e52377.
8. Wilson, D.N., N.I. Rao, and N.K. Reddy, *Concentration of Organo Chlorine pesticide residues in sediments from the Godavari River of East Godavari District of Andhra Pradesh.* Journal of Chemical, Biological and Physical Sciences (JCBPS), 2013. **3**(3): p. 2279.
9. Ateba, B., et al., *Occurrence of Salmonella spp in surface waters of Yaoundé, Cameroon.* J Environ Sci Water Resource, 2012. **1**: p. 243-50.
10. Venkatesan, K.D., M. Balaji, and K. Victor, *Microbiological analysis of packaged drinking water sold in Chennai.* International Journal of Medical Science and Public Health, 2014. **3**(4): p. 472-476.
11. Dacrory, S., K.H. Kamal, and S. Kamel, *EDTA-functionalized magnetic graphene oxide/polyacrylamide grafted carboxymethyl cellulose hydrogel for removal of Pb+ 2 from aqueous solution.* Journal of Polymers and the Environment, 2021: p. 1-14.
12. Ashmawy, S., et al., *Wastewater Treatment by Biological Filtration Technique Improves Biochemical and Microbiological Parameters in Nile tilapia (Oreochromis niloticus).* Journal of Basic and Environmental Sciences, 2024. **11**(4): p. 361-375.
13. Ashmawy, S., et al., *Investigation of metal accumulation and pathogenic bacterial loud in Nile tilapia farmed in treated water.* Water Science, 2025. **39**(1): p. 267-278.
14. Dacrory, S., *Development of mesoporous foam based on dicarboxylic cellulose and graphene oxide for potential oil/water separation.* Polymer Bulletin, 2022. **79**(11): p. 9563-9574.
15. Qasem, N.A., R.H. Mohammed, and D.U. Lawal, *Removal of heavy metal ions from wastewater: A comprehensive and critical review.* Npj Clean Water, 2021. **4**(1): p. 1-15.
16. Gholami Derami, H., et al., *A robust and scalable polydopamine/bacterial nanocellulose hybrid membrane for efficient wastewater treatment.* ACS Applied Nano Materials, 2019. **2**(2): p. 1092-1101.
17. Elsayed, G.H., S. Dacrory, and A.M. Fahim, *Anti-proliferative action, molecular investigation and computational studies of novel fused heterocyclic cellulosic compounds on human cancer cells.* International Journal of Biological Macromolecules, 2022. **222**: p. 3077-3099.
18. Dacrory, S., *Antimicrobial activity, DFT calculations, and molecular docking of dialdehyde cellulose/graphene oxide film against Covid-19.* Journal of Polymers and the Environment, 2021. **29**(7): p. 2248-2260.
19. Tappi, T., *Alpha-, beta-and gamma-cellulose in pulp.* TAPPI Standard Test Methods, 1999. **203**(1999): p. 5-9.
20. Dacrory, S., *Anti-proliferative, antimicrobial, DFT calculations, and molecular docking 3D scaffold based on sodium alginate, chitosan, neomycin sulfate and hydroxyapatite.* International Journal of Biological Macromolecules, 2024. **270**: p. 132297.
21. Patil, P., D. Sawant, and R. Deshmukh, *Physico-chemical parameters for testing of water–A review.* International journal of environmental sciences, 2012. **3**(3): p. 1194-1207.
22. Rice, E.W., et al., *Standard methods for the examination of water and wastewater.* 2012.
23. Dawwam, G.E., et al., *Bacteriological and Physicochemical Evaluation of Different Wells Water in El-Qalubia Governorate, Egypt.* Egyptian Academic Journal of Biological Sciences, G. Microbiology, 2023. **15**(1): p. 179-189.
24. Rice, E. and L. Bridgewater, *Association APH (eds)(2012) Standard methods for the examination of water and wastewater (Vol. 10).* American public health association, Washington, DC.
25. Holt, J.G., et al., *Bergey's Manual of determinate bacteriology.* 1994.
26. Dawwam, G.E., et al., *Production of the phytohormone Indole Acetic acid by some rhizospheric bacteria associated with the Egyptian flora.* Journal of Basic and Environmental Sciences, 2023. **10**(4): p. 130-137.

27. Biemer, J.J., *Antimicrobial susceptibility testing by the Kirby-Bauer disc diffusion method.* Annals of Clinical & Laboratory Science, 1973. **3**(2): p. 135-140.
28. Al-Shemy, M.T., et al., *Biocontrol of virulent Listeria monocytogenes using green carboxylated cellulose nanocrystals–silver nano-biohybrids.* International Journal of Biological Macromolecules, 2025. **290**: p. 139012.
29. El-Shall, F.N., A.M. Fahim, and S. Dacrory, *Making a new bromo-containing cellulosic dye with antibacterial properties for use on various fabrics using computational research.* Scientific Reports, 2023. **13**(1): p. 10066.
30. Mohamed-Ezzat, R.A., A.H. Hashem, and S. Dacrory, *Synthetic strategy towards novel composite based on substituted pyrido [2, 1-b][1, 3, 4] oxadiazine-dialdehyde chitosan conjugate with antimicrobial and anticancer activities.* BMC chemistry, 2023. **17**(1): p. 88.
31. Edition, F., *Guidelines for drinking-water quality.* WHO chronicle, 2011. **38**(4): p. 104-8.
32. Ayandiran, T., et al., *Microbial assessment and prevalence of antibiotic resistance in polluted Oluwa River, Nigeria.* The Egyptian Journal of Aquatic Research, 2014. **40**(3): p. 291-299.
33. Yu, J.M., et al., *High-performance electrochemical and photoelectrochemical water splitting at neutral pH by Ir nanocluster-anchored CoFe-layered double hydroxide nanosheets.* Nano Letters, 2023. **23**(11): p. 5092-5100.
34. Telo da Gama, J., et al., *Impact of different irrigation methods on the main chemical characteristics of typical mediterranean fluvisols in Portugal.* Agronomy, 2023. **13**(8): p. 2097.
35. Isnawati and G. Trimulyono. *Temperature range and degree of acidity growth of isolate of indigenous bacteria on fermented feed "fermege"*. in *Journal of Physics: Conference Series*. 2018. IOP Publishing.
36. Ateba, C.N., et al., *Occurrence of antibiotic-resistant bacteria and genes in two drinking water treatment and distribution systems in the North-West Province of South Africa.* Antibiotics, 2020. **9**(11): p. 745.
37. Cui, J., et al., *Engineering salt tolerance of photosynthetic cyanobacteria for seawater utilization.* Biotechnology Advances, 2020. **43**: p. 107578.
38. Liu, M., et al., *Impact of salinity on antibiotic resistance genes in wastewater treatment bioreactors.* Chemical Engineering Journal, 2018. **338**: p. 557-563.
39. Shoaib, M., et al., *A mini-review on commonly used biochemical tests for identification of bacteria.* International Journal of Research Publications, 2020. **54**(1): p. 1-7.
40. Abdeltawab, A.A., et al., *Bacteriological characterization of Salmonella species isolated from laying ducks.* Benha veterinary medical journal, 2018. **34**(1): p. 404-412.
41. Hussain, T., et al., *Biochemical characterization and identification of bacterial strains isolated from drinking water sources of Kohat, Pakistan.* African Journal of Microbiology Research, 2013. **7**(16): p. 1579-1590.
42. Al-Bayati, S.S., et al., *Isolation and identification of Pseudomonas aeruginosa from clinical samples.* Biochemical and Cellular Archives, 2021. **21**(2): p. 3931-3935.
43. Rawy, D.K., et al., *Isolation, characterization and identification of Klebsiella pneumoniae from assiut university hospital and sewage water in assiut governorate, Egypt.* Assiut Univ J Botany Microbiol, 2020. **49**(2): p. 60-76.
44. Janda, J.M., S.L. Abbott, and C.J. McIver, *Plesiomonas shigelloides revisited.* Clinical microbiology reviews, 2016. **29**(2): p. 349-374.
45. Mechergui, A., W. Achour, and A. Ben Hassen, *Comparison of 16S rRNA sequencing with biochemical testing for species-level identification of clinical isolates of Neisseria spp.* World Journal of Microbiology and Biotechnology, 2014. **30**(8): p. 2181-2188.
46. Banerjee, S., et al., *Detection and characterization of pathogenic Pseudomonas aeruginosa from bovine subclinical mastitis in West Bengal, India.* Veterinary world, 2017. **10**(7): p. 738.
47. Harakeh, S., H. Yassine, and M. El-Fadel, *Antimicrobial-resistant patterns of Escherichia coli and Salmonella strains in the aquatic Lebanese environments.* Environmental pollution, 2006. **143**(2): p. 269-277.
48. Kümmerer, K., *Antibiotics in the aquatic environment.* Antimicrobial resistance in the environment, 2011: p. 325-335.
49. Bezuidenhout, C.C., C.N. Ateba, and M. Mbewe, *Prevalence of Escherichia coli O157 strains in cattle, pigs and humans in North West Province, South Africa.* 2008.
50. Kinge, C.W. and M. Mbewe, *Characterisation of Shigella species isolated from river catchments in the North West province of South Africa.* South African Journal of Science, 2010. **106**(11): p. 1-4.
51. Talukdar, P.K., et al., *Antimicrobial resistance, virulence factors and genetic diversity of Escherichia coli isolates from household water supply in Dhaka, Bangladesh.* Plos one, 2013. **8**(4): p. e61090.
52. Mian, A.H., et al., *A study of bacterial profile and antibiotic susceptibility pattern found in drinking water at district Mansehra, Pakistan.* Applied Nanoscience, 2020. **10**: p. 5435-5439.
53. Schäfer, A., et al., *Physico-chemical water quality in Ghana: Prospects for water supply technology implementation.* Desalination, 2009. **248**(1-3): p. 193-203.
54. Moore, J.E., et al., *The presence of antibiotic resistant bacteria along the River Lagan.* Agricultural water management, 2010. **98**(1): p. 217-221.
55. Holappa, J., et al., *Antimicrobial activity of chitosan N-betainates.* Carbohydrate Polymers, 2006. **65**(1): p. 114-118.